TRENDS IN THE USE OF SOLID ROCKET MOTORS AND EFFECTS ON THE SPACE DEBRIS ENVIRONMENT

Sebastian Stabroth*, **Carsten Wiedemann**, **Peter Vörsmann**
Institute of Aerospace Systems, Technische Universität Braunschweig,
Hermann-Blenk-Str. 23, 38108 Braunschweig, Germany
*Corresponding author: phone: +49 531 391-9972; fax: +49 531 391-9966; email: s.stabroth@tu-bs.de

Michael Oswald
Astrium GmbH, Satellites, 88039 Friedrichshafen, Germany

Holger Krag, **Heiner Klinkrad**
Space Debris Office, ESA/ESOC, Robert-Bosch-Str. 5, 64293 Darmstadt, Germany

ABSTRACT

Typical solid rocket motors used for spacecraft orbital insertion burns generate slag and dust particles. The released particle clouds are distributed among different orbital regimes and lead to a number of impacts on other spacecraft surfaces.

The database of the ESA space debris model MASTER-2005 (Meteoroid and Space Debris Terrestrial Environment Reference) includes pre- and post-burn orbital data of performed solid rocket motor firings. The database also contains important information on propellant mass and motor types. An analysis of the generated table reveals that the firings can be divided into different manoeuvre classes: insertions into circular orbits, transfer orbits, and retro-firings, e.g. to initiate re-entry manoeuvres of return capsules.

Although the total number of solid rocket motor firings still increases, the annual firing rate shows a levelling-off during the recent years. The main reason for this changed trend is not a grown consciousness of the environmental problems caused by these motors. Instead, the use of liquid propellant engines as apogee kick stages gets more and more established. On the other hand, although the annual firing rate decreases, there is also a trend towards larger solid motors.

This paper analyses the latest trends in the use of solid rocket motors. It underlines the significant contribution such firings have on the space debris environment and gives impact risk predictions.

1. INTRODUCTION

While the application of solid rocket motors in lower stages or boosters is not able to position particles into Earth orbits, solid rocket motors (SRM) are in addition frequently employed at orbital altitudes as the final stage of satellite launch systems. They are either used for launch vehicle upper stages or occasionally built directly into the satellite itself.

Aluminium is used as an additive in the motor propellant of typical SRMs in order to increase performance and to dampen burn instabilities. The mass fraction of aluminium powder is 18% of the propellant mass on average.[1] During the burn process most of this aluminium is transformed into aluminium oxide. Assuming a stoichiometric combustion, the total mass fraction of Al_2O_3 is 34.6% of the propellant mass. Thus, in the exhaust gas of orbital SRM firings, a considerable amount of Al_2O_3 particles in the form of slag and dust is generally included and expelled into the space environment together with other combustion by-products, contributing to the space debris population.

The space debris model MASTER-2005 is able to simulate the release of SRM slag and dust particles and the resulting effects on the debris environment.[2]

2. PARTICLE RELEASE MODELLING

2.1 ESA-MASTER Model

The purpose of the MASTER space debris model is the realistic description of the orbital debris environment considering the contributions of both man-made objects and meteoroids. Using MASTER, it is possible to assess the impact risk for any given target orbit via flux predictions down to particle sizes of $1\,\mu$m. The model is based on the simulation of debris-generating events and their orbit evolution with time. The current model version, MASTER-2005, is considering 203 on-orbit fragmentations, 1,076 firings of solid rocket motors with the associated generation of slag and dust particles, and 16 releases of sodium-potassium coolant from Russian Radar Ocean Reconnaissance Satellite (RORSAT) reactors. In addition to these sources, the release of ejecta due to particle impacts on catalogued objects, the generation of surface degradation products (paint flakes) due to ultraviolet radiation and the interaction with atomic oxygen, and copper needles released during the West-Ford experiments are considered. The meteoroid model of Divine-Staubach and optional stream models according to Jenniskens/McBride and Cour-Palais are included as well.

MASTER-2005 was developed by the Institute of Aerospace Systems, Technische Universität Braunschweig, under ESA contract together with QinetiQ (UK), AIUB (Switzerland), and FGAN (Germany). During the last years, MASTER has become an internationally accepted tool with a growing user community in both research institutions and industry.

Although the purpose of MASTER is to give a long-term statistical estimation of the debris flux, the population generation tool of the MASTER developers branch software suite enables also a short-term simulation of the event-driven particulate environment.

2.2 SRM Firing Database

For a correct simulation of the SRM particle exhaust mechanism, knowledge of the orientation of the motor axis is necessary. Hence, the complete pre- and post-burn orbital data of every performed SRM firing had to be collected and a database also containing important information on propellant mass and motor name had to be compiled. The database established for MASTER-2005 contains 1,076 entries before the reference epoch of May 2005, where events not producing particles with a stable orbit are neglected.

The MASTER-2005 firing database was recently updated with information on a large number of orbital SRM retro-burns of Russian return capsules.[3,4] Objects released by those firings reach highly eccentric orbits with perigees in the lower regions of the atmosphere. Thus, they produce no long-term effect on the debris environment. However, the large number of those firings between 1970 and 1990 contributes to the debris flux during this historical time frame in addition to the firings included with MASTER-2005.

Fig. 1 shows the annual number of orbital SRM firings as included in the established firing database which now comprises 1,845 firings altogether. The annual number of SRM firings reached a maximum during the 1980s with more than 80 firings per year. The firing rate has declined since then reaching a minimum of seven orbital SRM burns in 2002, the lowest number since the use of orbital SRMs for space applications.

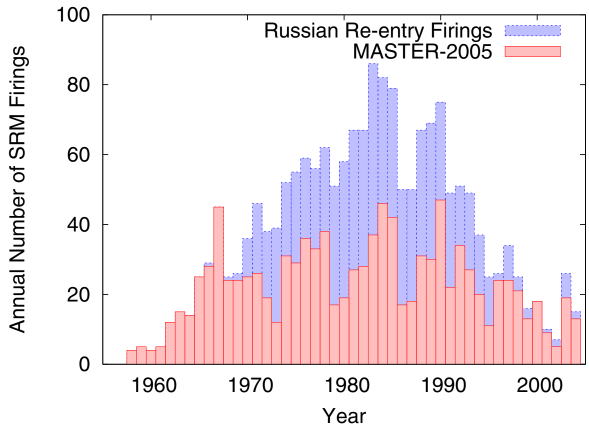

Figure 1. Annual number of orbital SRM firings.

The debris population simulated with MASTER and propagated forward in time is validated against cumulated flux measurements from returned spacecraft surfaces that had been exposed to the debris environment for a long time period, i.e. Long Duration Exposure Facility (LDEF), the European Retrievable Carrier (EuReCa), and the solar cells of the Hubble Space Telescope (HST).[5,6]

2.3 SRM Slag

Investigations have been made in the past concerning the ejection of slag particles from SRMs after passing the nozzle throat, particularly after burn-out. As a result of measurement data, two slag ejection models exist for the time being – one approach by NASA and one by the MIT/Lincoln Laboratory (MIT/LL). The two slag ejection models are based on different observation techniques. The approach by NASA was derived from optical observations of statically fired SRMs, originally described by Siebold et al.[7] and Anderson et al.[8] In contrast, the MIT/LL law as described by Bernstein and Sheeks[9] is based on the observation of ascending sub-orbital launch vehicles using ground-based radar devices and infrared telescopes. While the ground tests involved STAR-48 and STAR-63 motors with propellant masses of 2,000 kg and 3,700 kg respectively, the radar observations refer to a four-nozzle engine design loaded with 1,680 kg of propellant. Both models are restricted to particle diameters above 5 mm due to measurement limitations. The largest objects observed by MIT/LL radar measurements are believed to have diameters of about 3 cm.

For the implementation in MASTER-2005, the size distribution of objects larger than a threshold diameter of 5 mm is a combination of both NASA and MIT/LL models. The observed cumulative object numbers and ranges are scaled to the propellant mass of a STAR-37 reference motor with 700 kg propellant mass and assuming a baseline of 1,800 particles greater than 5 mm, which is a compromise with the aim to meet measurement data. The number distribution is proportional to $1/d^3$, hence follows a $1/m$ relationship displayed in Fig. 2.

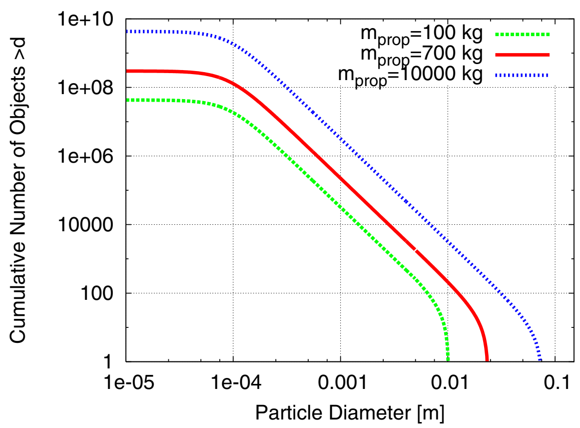

Figure 2. Cumulative SRM slag size distribution as used in MASTER-2005.[2]

There are no clues yet for the distribution of diameters below the 5 mm observation threshold. The number of these sub-millimetre slag objects released during one burn may be very high, while the contribution of these objects to the totally ejected slag mass remains rather low. For the purpose of the MASTER-2005 model, the extension of the size distribution is a steady continuation of the relation used for particle sizes above 5 mm reaching a maximum at 100–150 μm, the size of particles that impacted Space Shuttle windows.[10] The upper tail-off of the parameterised size distribution depends on the motor size as shown in Fig. 2 for exemplary engines.

It is assumed that 50% of the particles are created from propellant material (Al_2O_3 density 3.5 g/cm^3) and 50% are created from liner material (density 1.8 g/cm^3), which is used to fix the solid propellant on the insulation layer. 5% of Al_2O_3 slag mass are assumed to be ejected during the last quarter of an SRM burn while the majority is assumed to be generated after burn-out (95% of Al_2O_3 slag mass).

The ejection velocity has been adopted from the NASA approach, because of the more reliable measurement installation used to obtain the ground test data underlying this model. The ejection velocity of the generated objects is set to a constant value of 75 m/s. The ejection angle plays only a minor role within the model, because of the low resulting radial velocities. A review of the cone angle of SRM nozzles revealed that an exhaust cone angle of 20° is a representative value.

2.4 SRM Dust

In addition to larger slag particles, small dust particles of less than 1 μm up to more than 10 μm in size are generated continuously during a burn and expelled through the nozzle of orbital SRMs.[11]

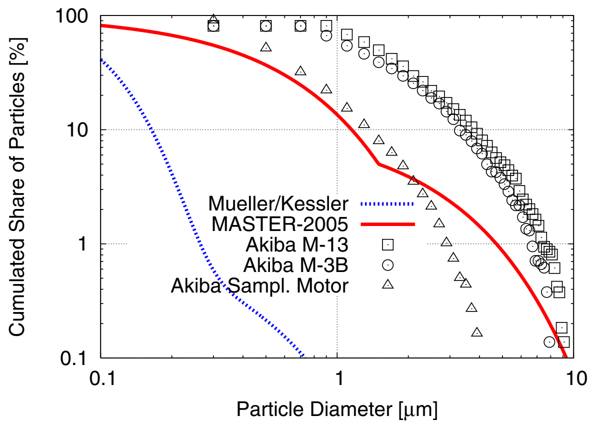

Figure 3. Normalised SRM dust size distribution as used in MASTER-2005 in comparison with measured distributions from the literature.[2,11,12]

The generation of micrometer-sized dust is handled in MASTER-2005 along with the models governing the generation of several additional debris populations. The current model version MASTER-2005 uses a mean size and velocity distribution for SRM dust that is derived from measured distributions given in the literature,[11,12] see Fig. 3 and 4.

For the angular distribution of the particles leaving the motor nozzle, rotational symmetry is assumed with a limiting cone angle, which is the limiting half-angle of the cone formed by the exhaust plume. The model formulation in MASTER-2005 follows the approach established by Mueller and Kessler.[11] The maximum exit angle depends on particle size and can be approximated analytically by a bi-modal exponential function. The fit to the original data is shown in Fig. 5. The distribution of the actual exit angle within this cone is not uniform, but instead follows a plume shape factor giving more emphasis to exit angles near the motor centre line.

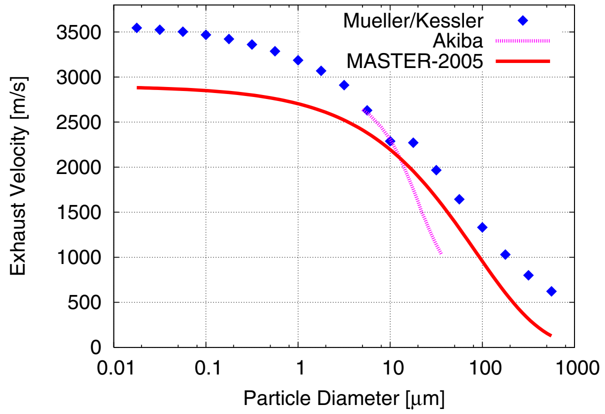

Figure 4. SRM dust velocity distribution as used in MASTER-2005 in comparison with measured distributions from the literature.[2,11,12]

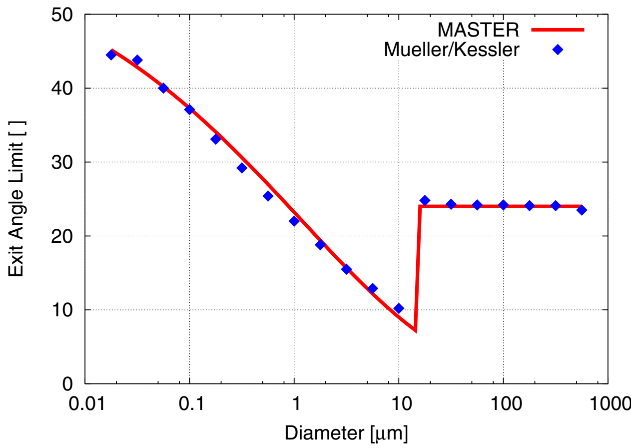

Figure 5. Bi-modal analytical fit used in MASTER-2005 for the exit angle limit postulated by Mueller and Kessler.[11]

3. SRM FIRING ANALYSIS

The analysis of the generated database reveals that SRM firings can be divided into different manoeuvre classes: low altitude orbital insertions, transfer orbit insertions, high altitude apogee kick burns, and re-entry firings. In Fig. 6, the apogee altitude of each final orbit is plotted against its perigee altitude. Firings which lead to circular orbits thus can be found on the diagonal. The cluster of circular orbits in the upper right part of the diagram can be attributed to the U.S. Vela satellite program which was dedicated to the detection of atmospheric nuclear tests. Another broad cluster of SRM firings into a circular orbit is made up by the large number of GEO insertion firings. At the same apogee altitude, but at lower perigee altitudes, insertions into the corresponding transfer orbits using solid upper stages are clearly visible. A similar SRM activity can be observed for the U.S. Navstar (GPS) program around 20,000 km altitude. In the lower left part of the diagram, the common application of SRMs also for the various types of LEO missions is documented. The vertical stripe at low perigee altitudes is caused by several re-entry manoeuvres performed by Russia and China, where a theoretical perigee altitude below 50 km for the resulting orbit was assumed.

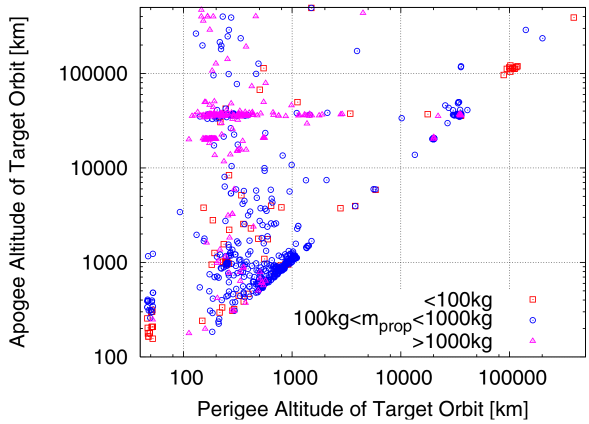

Figure 6. Apogee and perigee altitude of SRM firing target orbits. The motor size is separated into three different propellant mass classes.

SRMs with propellant masses larger than 1,000 kg are mainly used for transfer orbit insertions into GTO and GPS transfer orbits as can be derived from the mass classes displayed in Fig. 6. Motors with propellant masses less than 100 kg are often dedicated to special missions (re-entry firings, orbital insertion of the above mentioned Vela satellites). The SRM propellant mass class between 100 kg and 1,000 kg contributes throughout all target orbit regions with an emphasis on LEO missions and GEO/GPS apogee kick insertions.

A differentiation with respect to the target orbit's inclination in Fig. 7 shows that a large amount of the total number of SRM firings can be attributed to insertions into GEO with 0° inclination, GTO in the 22°–30° inclination band, and sun-synchronous orbit (SSO) at 98° inclination. The inclination peaks due to the Russian photo-reconnaissance satellites are visible between 60° and 80°. The peak in the MASTER-2005 data at 60° inclination is due to a number of

SRM firings of Russian RORSATs into disposal orbits between 900 km and 950 km altitude as well as due to re-entry firings of Chinese photo-reconnaissance satellites.

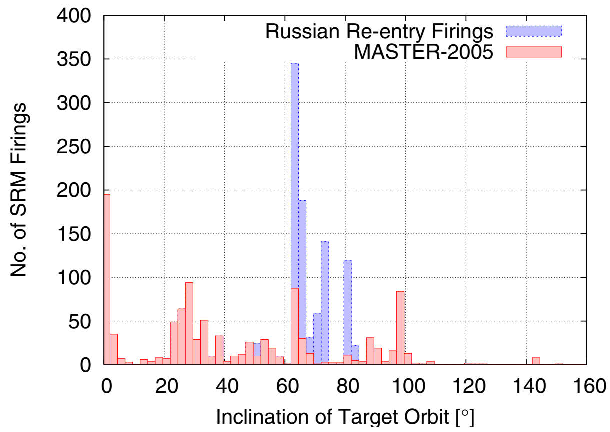

Figure 7. Number of SRM firings vs. target orbit inclination.

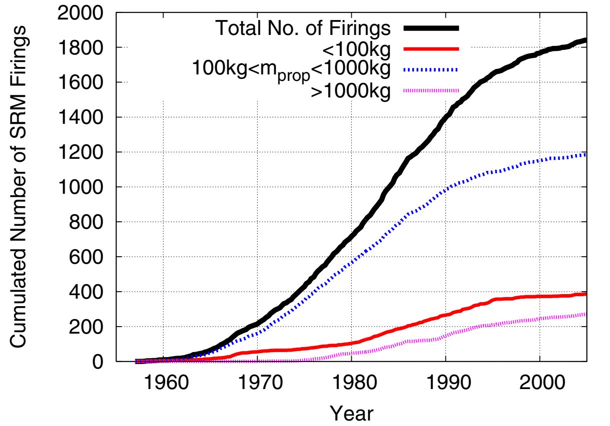

Figure 8. Total number of orbital SRM firings.

Fig. 8 shows the total number of orbital SRM firings. The number of firings still increases. However, a clear levelling-off since 1990 can be observed. This changed trend is not related to an awareness of the environmental problems caused by the orbital operation of SRMs. Instead, the reduction in the annual number of SRM firings can be attributed to the increased use of combined bi-propellant engines, especially for orbit insertions into GEO.

Most satellites launched into GEO during the past decades used an integrated apogee motor to perform final insertion from GTO into the GEO ring. SRMs were preferred for the orbit insertion because of their low complexity and high reliability. However, during the last decade, it became more and more common to use the satellite on-board bi-propellant reserve in combination with a larger 400 N thruster to apply the apogee kick instead of the formerly predominating SRMs. The reduction in the number of annual GEO insertion firings with SRMs is shown in Fig. 9. At the end of the 1980s, between 10 and 15 GEO insertions with SRMs were performed. This firing rate has since then decreased to less than two per year. The use of liquid propellant simplifies the system integration since only one independent thrust system has to be implemented. In the future almost every GEO satellite can be expected to use an internal liquid apogee kick motor. Liquid engines offer a more exact orbit insertion than SRMs that can only be ignited once and burn up all propellant available. With a more exact insertion, more fuel is remaining for the orbit control of the satellite in normal operations.

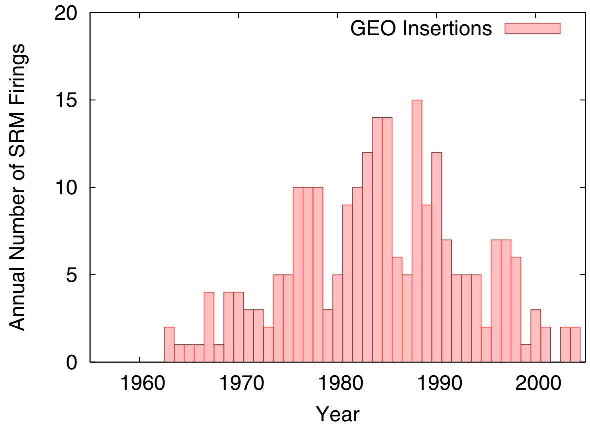

Figure 9. Annual number of GEO insertion firings with SRMs.

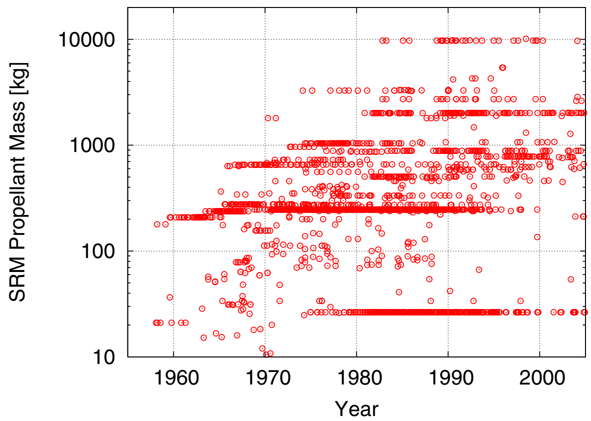

Figure 10. SRM propellant mass of performed orbital firings vs. time.

On the other hand, Fig. 10 shows that, although the number of orbital SRM firings decreases, there is also a trend towards larger engines. The amount of satellite launches with the aid of the Inertial Upper Stage (IUS) since 1982 contributed significantly to the total slag population due to the very large propellant masses involved (9,700 kg for the IUS lower stage motor ORBUS-21, 2,700 kg for the IUS upper stage motor ORBUS-6). For the orbital insertion of GPS satellites into their transfer and final orbits STAR-48 and STAR-37 motors are used with propellant masses of 2,000 kg and 900 kg, respectively. The STAR-30 motor often used for insertion of telecommunication satellites into GEO has a propellant mass of 500-600 kg. In contrast to these firings of motors with larger propellant masses, SRM firings with low propellant masses of up to 100 kg have disappeared as shown in Fig. 10, with one exception. The orbital SRM retro-burns of Russian film return capsules with an estimated 26 kg propellant mass are since the mid-1970s still in use today, though with a lower operational frequency.[3,4]

Most of the solid rocket motor flights have been performed by the USA and Russia. Russia's share on the total number of SRM firings is high, but only due to the large amount of capsule re-entry firings. If the Russian re-entry firings are neglected, less than one third of the orbital SRM firings can be attributed to other nations, among them Japan, or to international organisations like INTELSAT or INMARSAT. The share of Japanese firings is steadily decreasing, obviously due to the appearance of the cryogenic H-2 launcher. China and Europe do not contribute significantly to the SRM statistics. Few insertions of payloads into GEO have been performed with SRMs. Latest tendencies show that the use of liquid propellant motors as apogee kick motors gets more and more established also in these countries.

4. EFFECTS ON THE ENVIRONMENT

4.1 Simulation of Particle Releases

Based on the established firing database, an entire simulation of each firing event and the propagation of each SRM particle cloud with time was performed. The debris population generation tool of MASTER-2005 was used for this purpose.

As the exhaust velocities for small dust particles are quite high (1–4 km/s) in relation to the velocity of slag particles, the parent's orbital velocity is often neutralised, so that most of the dust particles decay immediately. This circumstance is visualised by the Gabbard diagram in Fig. 11 for the circularisation burn of a satellite into sun-synchronous orbit at 730 km altitude. The trajectory of the resulting dust particles is sub-orbital with a theoretical perigee below the surface of Earth. SRM dust therefore re-enters the Earth's atmosphere immediately. Only larger slag objects released at the end or after SRM burn-out are predicted to reach Earth orbit and thus contribute to the debris environment.

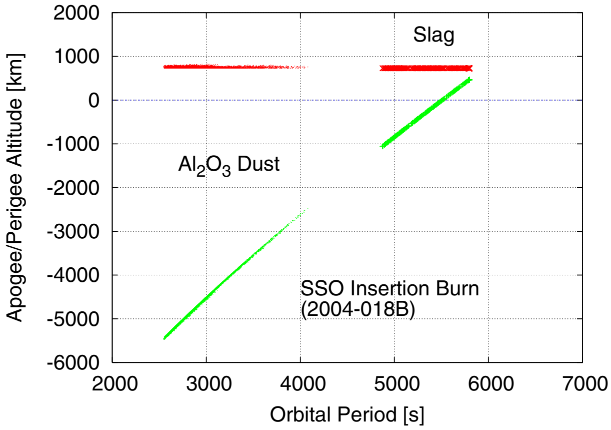

Figure 11. Gabbard diagram of a circularisation burn into sun-synchronous orbit at 730 km altitude. Displayed are the released clouds of dust and slag particles with their initial apogee and perigee altitudes.

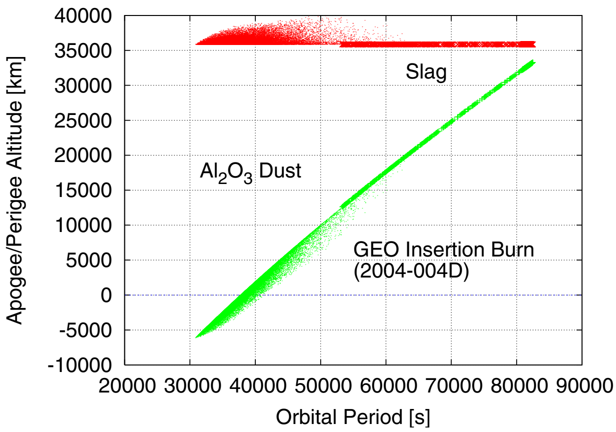

Figure 12. Gabbard diagram of a circularisation burn into GEO at 35,786 km altitude. Displayed are the released clouds of dust and slag particles with their initial apogee and perigee altitudes.

In contrast to LEO firings, apogee kick burns at high altitude are often combined with a change in inclination, especially for GEO insertions. Since these burns have a significant out-of-plane component, and since some particles leave the engine at high angles relative to the centre line, most of the SRM dust particles are inserted into eccentric orbits which do not immediately re-enter. The resulting orbits are displayed by the Gabbard diagram in Fig. 12. Observed impact craters on LDEF experiment trays and HST surfaces with aluminium and oxygen content are assumed to be caused by such particles.[5,13,14]

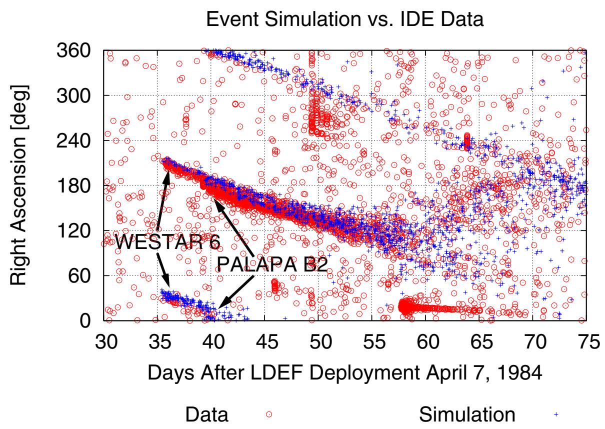

Figure 13. LDEF location at the time of measured impacts as recorded by the IDE sensors vs. geocentric right ascension. The distinct measurement signature is compared to a simulation of SRM particle impacts caused by two SRM firings of the satellites WESTAR 6 and PALAPA B2.[15]

A direct confirmation of particle impacts onto satellite surfaces due to SRM firings could be found for the LDEF Interplanetary Dust Experiment (IDE) data which shows signatures of particle clouds that intersect the orbit of LDEF. The simulation of firings and a close encounter analysis of the released objects with LDEF's orbital path related SRM firings of the satellites WESTAR 6 and PALAPA B2 to the observed measurement signature – in the literature referred to as the "May Swarm". Fig. 13 shows the comparison of the impact signature with the firing event simulation in terms of the timely spread impact location. Details on the event simulation can be found in Stabroth et al.[15] The findings underline the strong contribution SRM burns pose to the debris environment.

4.2 Historical Evolution of the Environment

Based on the semi-deterministic model architecture of MASTER-2005, it is possible to display the historical evolution of the debris population. Changes to the environmental state are made not only by debris generating events itself but also by disturbing forces continuously altering the orbital motion of the released particles with time. The object distribution of a population at a certain size threshold can be displayed by spatial density distributions.

Fig. 14 shows the simulated evolution of the debris density in LEO between 1960 and 2005 for all objects larger than 1 mm as an example. At this size threshold in LEO, SRM firing remnants orbit the Earth with roughly the same quantity as fragmentation debris. For both sources, the combined effect of the rate in which particles are generated and the rate in which particles are removed out of orbit due to atmospheric drag is visible. The first increase in SRM spatial density is due to the increase in the number of firings at the end of the 1960s. The annual number of SRM particles generated in the early 1970s is compensated by a maximum in solar activity and thus higher atmospheric densities at this time. Further on, the SRM density increases due to the decreasing solar activity and reaches a first maximum at the end of the 1970s. Here, the density peak reduces at first because of the following solar cycle but increases again due to the larger number of SRM burns in the 1980s. The next solar cycle compensates the density increase reaching a maximum at the same level as the decade before. Since the annual number of firings strongly minimises between 1990 and 2000, a third density peak at the mid-1990s degrades towards 2005.

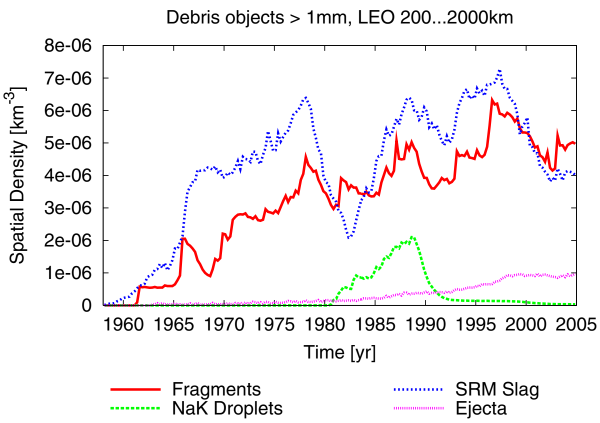

Figure 14. Historical evolution of the debris environment in LEO for objects larger 1 mm. Contributions from different source terms are shown.

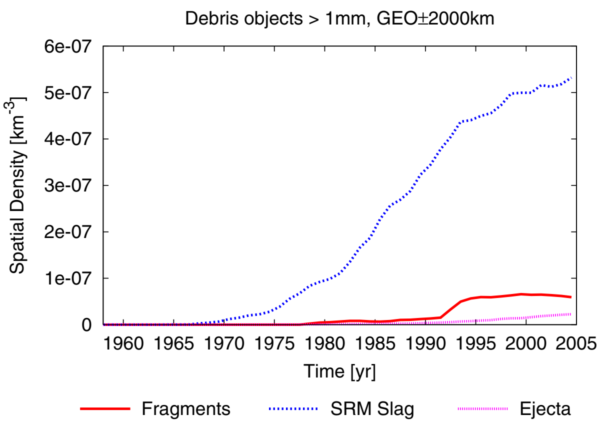

Figure 15. Historical evolution of the debris environment in GEO for objects larger 1 mm. Contributions from different source terms are shown.

A completely different situation is observed for the

GEO environment as an outcome of the simulation. Fig. 15 shows the time-evolution of debris objects larger than 1 mm in GEO±2,000 km. The debris environment at this size threshold is dominated by SRM firing remnants due to the comparatively low number of fragmentations in GEO. Since the altitude of GEO is far beyond the outer regions of the Earth's atmosphere, every object launched into GEO or set free there will remain in the orbit's vicinity forever. This explains the increase in SRM slag spatial density as displayed in Fig. 15. The density curve follows the cumulation of the annual number of GEO insertions with solid rocket motors (compare with Fig. 9). Due to the highest number of GEO insertions during the 1980s, the density increases with a steep gradient. The accumulation of slag objects levels off because of the lower number of annual SRM firings since the mid-1990s.

4.3 Current Impact Risk

The MASTER-2005 flux calculation tool is able to derive the background impact flux for various target orbits, surface orientations, and time. This flux browser analyses the pass of the simulated debris population through an Earth-centred volume discretisation grid. If particles interfere with the target volume, the flux contributions of the passes are evaluated. The total resulting flux is cumulated until the pre-calculated reference spatial density as given above is reached. Based on this method, the impact flux on targets in different orbital environments can be derived.

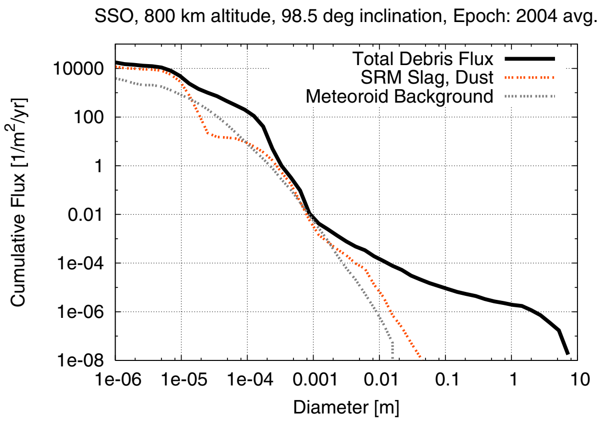

Figure 16. MASTER-2005 flux comparison for the year 2004 at 800 km sun-synchronous orbit vs. impactor diameter.

In order to show the influence of orbital SRM firings on the debris environment, flux predictions for two reference orbits are presented: a sun-synchronous orbit in LEO and the geostationary orbit. Fig. 16 and 17 display the average cumulative debris flux distribution versus impactor diameter for the year 2004 as modelled in MASTER-2005 assuming a spherical target.

Since all debris objects on near-polar orbits have to share the same small volume element at high declinations, the spatial density is significantly increased at the polar regions. In addition, the highest spatial density is reached in altitudes of 800 and 1,400 km.[2] Therefore, the highest collision risk is connected to the sun-synchronous orbit in 800 km altitude, see Fig. 16. According to the model, the current total debris flux in this orbit often used for Earth observation missions can reach and even exceed the meteoroid background in the diameter regime below 100 μm. SRM firing remnants make up a large part of the total debris flux at the millimetre (slag) and smaller than 10 μm diameter (dust) region.

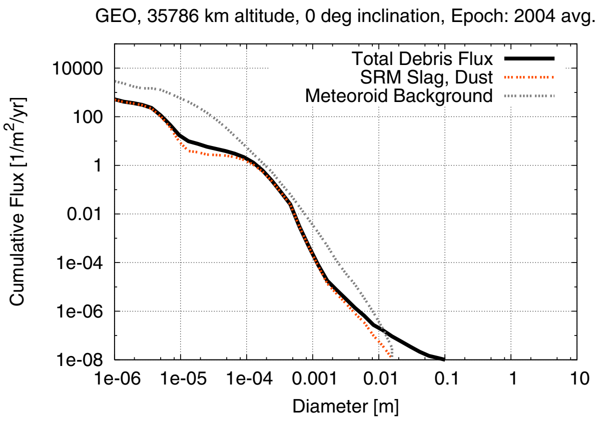

Figure 17. MASTER-2005 flux comparison for the year 2004 at GEO altitude vs. impactor diameter.

The impact flux is significantly lower for GEO as presented in Fig. 17. According to MASTER-2005, the average background of debris impacts remains below the natural flux of micro-meteoroids. However, the total debris flux almost exclusively originates of SRM slag and dust objects.

4.4 Future Evolution

The future evolution of the orbital debris environment strongly depends upon the assumptions made with regard to the future launch activity and the measures taken by the international community to mitigate the orbital debris problem.

Different future scenarios regarding the use of solid rocket motors are possible. However, it can be expected that SRM circularisation burns in LEO are continuously performed with smaller launch vehicles like SHAVIT, PEGASUS, MINOTAUR, or the future European VEGA launcher. In contrast, the IUS with its large perigee kick motor performed a final mission in 2004 and is not going to be used in the future according to Boeing.[16]

For the purpose of the MASTER-2005 model, the best and worst implementation of debris mitigation measures with no significant variation in future traffic rates are assumed. Regarding SRM firings they are described as follows:

- Business as usual: SRM firing traffic based on the last eight years of activity
- SRM firing prevention: Traffic reduction from 2015 on, reaching 5% of current levels by 2025.

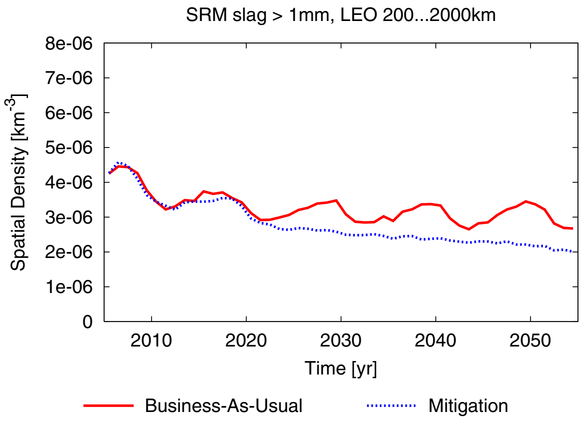

Figure 18. Future evolution of the debris environment in LEO for objects larger than 1 mm according to MASTER-2005. Only the contribution from SRM slag objects is shown.

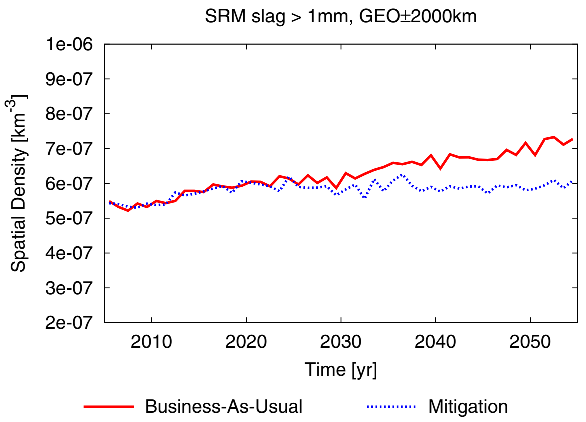

Figure 19. Future evolution of the debris environment in GEO for objects larger than 1 mm according to MASTER-2005. Only the contribution from SRM slag objects is shown.

It is interesting to note that the population of SRM slag particles larger than 1 mm in LEO declines even in the business-as-usual scenario, see Fig. 18. The traffic model used for MASTER-2005 is based on the last eight years of activity and therefore reflects the fact that fewer SRM firings have taken place in recent years. The number of generated SRM objects in the future is over-compensated by the self-cleaning effect of the atmosphere in LEO. The atmospheric influence is further driven by the future solar cycles which can be distinguished in Fig. 18.

In contrast to the LEO environment, the population of SRM slag particles larger than 1 mm in GEO increases in the business-as-usual scenario, see Fig. 19. Assuming the last eight years of SRM activity as the baseline for the future traffic, the GEO population of SRM slag objects will increase by 40% during the next 50 years. Only the introduction of SRM slag prevention in the mitigation scenario effectively stabilises the SRM slag population in the GEO region.

5. SUMMARY

Typical solid rocket motors used for spacecraft orbital insertion burns generate slag and dust particles. The released particle clouds contribute to the debris environment and lead to a number of impacts on spacecraft surfaces. The impact flux of SRM particles is a strong contributor to the total debris flux and has to be accounted for in the risk assessment of current and future satellite missions.

For the simulation of the debris environment caused by SRM burns, a firing database was established which includes historical pre- and post-burn orbital data of the performed engine firings. The database also contains important information on propellant mass and motor types. While SRMs are still in use today, the annual firing rate shows a levelling-off during the recent years. The main reason for this changed trend is the predominant use of re-ignitable liquid propellant engines as apogee kick stages which get more and more established, especially for orbit insertions into GEO.

Assuming an ongoing SRM traffic based on the last eight years of activity, the consequence for the future debris environment is that the SRM slag population will slowly decline in LEO due to atmospheric drag. However, the environment can only be stabilised also in the GEO region if SRM firing prevention is taken into account as a mitigation measure.

References

[1] Wegener, P., Krag, H., Rex, D., Bendisch, J., Klinkrad, H., *The Orbital Distribution and Dynamics of Solid Rocket Motor Particle Clouds for an Implementation into the MASTER Debris Model*, Adv. Space Res. 23, pp. 161–164, 1999

[2] Oswald, M., Stabroth, S., Wegener, P., Wiedemann,

C., Martin C., Klinkrad, H., *Upgrade of the MASTER Model*, Final Report of ESA contract 18014/03/D/HK(SC), Institute of Aerospace Systems, April 2006

[3]Stabroth, S., Homeister, M., Oswald, M., Wiedemann, C., Klinkrad, H., Vörsmann, P., *The Influence of Solid Rocket Motor Retro-Burns on the Space Debris Environment*, paper PEDAS1-0015-06, 36$^{\text{th}}$ COSPAR Scientific Assembly, Bejing, China, July 2006

[4]Wiedemann, C., Homeister, M., Oswald, M., Stabroth, S., Klinkrad, H., Vörsmann, P., *Additional Historical Solid Rocket Motor Burns*, paper IAC-06-B6.2.07, 57$^{\text{th}}$ International Austronautical Congress, Valencia, Spain, October 2006

[5]Anon., *Meteoroid and Debris Flux and Ejecta Models*, Final Report of ESA Contract No. 11887/96/NL/JG, Unispace Kent, ESA 1999

[6]Anon., *Post-Flight Impact Analysis of HST Solar Arrays – 2002 Retrieval*, Final Report of ESA Contract No. 16283/NL/LvH, UniSace Kent (UK), ONERA (FR), Natural History Museum (UK), 2005

[7]Siebold, K.H., Matney, M.J., Ojakangas, G.W., Anderson, B.J., *Risk Analysis of 1–2 cm Debris Populations from Solid Rocket Motors and Mitigation Possibilities for Geotransfer Orbits*, Proceedings of the First European Conference on Space Debris, ESA SD-01, Darmstadt, Germany, April 1993

[8]Anderson, B.J., Ojakangas, G.W., Anz-Meador, P.D., *Solid-Rocket-Motor Contribution to Large-Particle Orbital Debris Population*, Journal of Spacecraft and Rockets, Vol. 33, No. 4, pp. 513ff., 1996

[9]Bernstein, M.D., Sheeks, B.J., *Field Observation of Medium-sized Debris from Postburnout Solid-fuel Rocket Motors*, International Symposium on Optical Science, Engineering, and Instrumentation (SPIE), paper 3116-32, Proceedings of SPIE, Vol. 3116, 1997

[10]Jackson, A., Bernhard, R., *Large Solid Rocket Motor Particle Impact on Shuttle Window*, The Orbital Debris Quarterly News, Vol. 2, Issue 2, pp. 3–4, April–June, 1997

[11]Mueller, A.C., Kessler, D.J., *The Effects of Particulates from Solid Rocket Motors Fired in Space*, Adv. Space Res., Vol. 5, No. 2, pp. 77–86, 1985.

[12]Akiba, R., Inatani, Y., *Behavior of Alumina Particle Exhausted by Solid Rocket Motors*, Proceedings of the Workshop on Space Debris, Kanagawa, Japan, May 11, 1989, Institute of Space and Astronautical Science (ISAS), Report SP No. 11, ISSN 0288-433X, pp. 51–59, Kanagawa, Japan, March 1990.

[13]Graham, G.A., McBride, N., Kearsley, A.T., Drolshagen, G., Green, S.F., McDonnell, J.A.M., Grady, M.M., Wright, I.P., *The Chemistry of Micrometeoroid and Space Debris Remnants Captured on Hubble Space Telescope Solar Cells*, International Journal of Impact Engineering, Vol. 26 (2001), pp. 263–274, 2001

[14]Wegener P., *Modelling and Validation of the Space Debris Flux onto Satellites*, *ZLR Forschungsbericht 2004-02*, Center of Aerospace Technology, Braunschweig, Shaker Verlag Aachen, 2004

[15]Stabroth, S., Oswald, M., Wiedemann, C., Klinkrad, H., Vörsmann, P., *Explanation of the May Swarm signature in the LDEF IDE impact data*, Aerospace Science and Technology 11, pp. 253–257, 2007

[16]Anon., *Boeing: History – Products - Boeing Inertial Upper Stage*, http://www.boeing.com/history/boeing/ius.html, last access: July 2007